

XAS and XMCD studies of magnetic properties modifications of Pt/Co/Au and Pt/Co/Pt trilayers induced by Ga⁺ ions irradiation

Piotr Mazalski,^a Iosif Sveklo,^{a*} Zbigniew Kurant,^a Katharina Ollefs,^b Andrei Rogalev,^b Fabrice Wilhelm,^b Juergen Fassbender,^c Lech Tomasz Baczewski,^d Andrzej Wawro^d and Andrzej Maziewski^a

Received 19 November 2014

Accepted 11 February 2015

Edited by S. Svensson, Uppsala University, Sweden

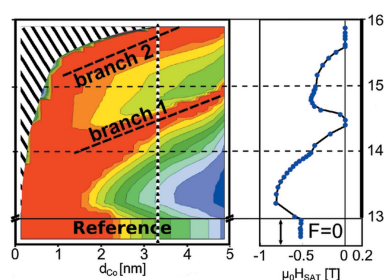
Keywords: magnetic and magneto-optical properties; trilayer; X-ray magnetic circular dichroism (XMCD) spectra; perpendicular magnetic anisotropy.

^aFaculty of Physics, University of Białystok, Ciołkowskiego 1L, Białystok 15-245, Poland, ^bEuropean Synchrotron Radiation Facility, BP 220, F-38043 Grenoble, France, ^cInstitute of Ion Beam Physics and Materials Research, Helmholtz-Zentrum Dresden-Rossendorf, PO Box 510119, Dresden 01314, Germany, and ^dInstitute of Physics, Polish Academy of Sciences, Al. Lotników 32/46, Warszawa 02-668, Poland. *Correspondence e-mail: jo@uwb.edu.pl

Magnetic and magneto-optical properties of Pt/Co/Au and Pt/Co/Pt trilayers subjected to 30 keV Ga⁺ ion irradiation are compared. In two-dimensional maps of these properties as a function of cobalt thickness and ion fluence, two branches with perpendicular magnetic anisotropy (PMA) for Pt/Co/Pt trilayers are well distinguished. The replacement of the Pt capping layer with Au results in the two branches still being visible but the in-plane anisotropy for the low-fluence branch is suppressed whereas the high-fluence branch displays PMA. The X-ray absorption spectra and X-ray magnetic circular dichroism (XMCD) spectra are discussed and compared with non-irradiated reference samples. The changes of their shapes and peak amplitude, particularly for the high-fluence branch, are related to the modifications of the local environment of Co(Pt) atoms and the etching effects induced by ion irradiation. Additionally, in irradiated trilayers the XMCD measurements at the Pt *L*_{2,3}-edge reveal an increase of the magnetic moment induced in Pt atoms.

1. Introduction

Ultrathin magnetic films, multilayered systems and nanostructures with perpendicular magnetic anisotropy (PMA), which consist of alternating magnetic and nonmagnetic layers, attract much attention due to the fundamental research of nanomagnetism and their technological applications in memory, spintronics and magnetic logic devices. Effective magnetic anisotropy is a result of the interplay of magneto-crystalline, magnetoelastic, surface (interface) and shape anisotropy contributions (Chowdhury *et al.*, 2012). In systems containing ultrathin magnetic layers, PMA is often dominated by interfacial anisotropy (Stillrich *et al.*, 2010; Knepper & Yang, 2005). Magnetic anisotropy energy in such structures might exceed the respective value for bulk material by an order of magnitude (Lehnert *et al.*, 2010). The structure and the quality of interfaces are the factors of crucial importance that affect effective anisotropy. For very thin films, PMA can be enhanced by the suppression of interface diffusion (Bandiera *et al.*, 2012) which is responsible for interface mixing (Lee *et al.*, 2013) or by the interface roughness (Schaller *et al.*, 1999). Contributions from the bottom and the upper interfaces to the magnetic anisotropy are not equivalent (Bandiera *et al.*, 2011). Therefore, the resulting anisotropy depends on the fabrication techniques (Lee *et al.*, 2013) and growth conditions such as the type of seed layer (Stillrich *et al.*, 2010) or the growth temperature (Mihai *et al.*, 2013).



Although PMA was discovered in Au/Co multilayers (Chappert & Bruno, 1988), the Pt/Co system is one of the most intensively studied owing to the enhanced magneto-optical response in the ultraviolet range (Brandle *et al.*, 1992). The structure and the interface alloying have significant influence on the magnetic and magneto-optical properties and can be used as adjustment parameters (Poulopoulos *et al.*, 2003). Various other approaches have been considered to further improve the properties relevant to applications, *e.g.* doping of the interfaces in order to oxidize Co atoms (Zhang, Yang *et al.*, 2013; Zhang, Wu *et al.*, 2013; Manchon *et al.*, 2008; Nistor *et al.*, 2011) or the insertion of ultrathin layers, which are immiscible with both Pt and Co, in order to suppress interdiffusion (Bandiera *et al.*, 2012).

The local environment and the coordination play important roles for the magnetic properties of Co atoms. The enhanced magnetic susceptibility of Pt(Pd) atoms leads to an effective interlayer exchange coupling in multilayers compared with a system containing smaller spin-orbit coupling like Cr or Cu.

The electronic structure of the nonmagnetic components plays an important role in the anisotropy and the coupling between magnetic components of nanostructures exhibiting PMA. In granular Pt/Co multilayers the Co particles are coupled ferromagnetically (Bartolome *et al.*, 2007). The separating Pt layers are involved in the interparticle exchange coupling by polarization of the Pt atoms due to hybridization of the Pt *5d* and the Co *3d* electrons. Oscillatory interlayer coupling between the Co layers is attributed to the Ruderman–Kittel–Kasuya–Yosida interactions. It is concluded that the magnetic polarization of the Pt atoms is responsible for this behavior (Knepper & Yang, 2005).

Local irradiation of the continuous Pt/Co multilayers with an ion beam or focused ion beam (FIB) is a powerful tool for nanostructure fabrication (Chappert *et al.*, 1998; Rettner *et al.*, 2002; Vieu *et al.*, 2002; Kuswik *et al.*, 2011). Ion bombardment destroys a sharp chemical profile at the interfaces in the as-grown layered films. Suppression of PMA followed by re-orientation to the in-plane alignment was demonstrated upon irradiation for Pt/Co multilayers with 30 keV He⁺ ions (Chappert *et al.*, 1998; Fowley *et al.*, 2013). The opposite effects have also been reported very recently (Maziewski *et al.*, 2012; Jaworowicz *et al.*, 2009; Mazalski *et al.*, 2013). The possibility of multiple changes of the magnetization orientation between in-plane and out-of-plane directions in Pt/Co/Pt trilayers induced by ion irradiation has been demonstrated. Consecutive states with PMA separated by an in-plane magnetization phase were induced in in-plane magnetized as-grown trilayers with increasing fluence of ions. In the two-dimensional maps of magnetic and magneto-optical properties as a function of d_{Co} (cobalt thickness) and F (ion fluence), two elongated PMA regions, in shapes resembling ‘branches’, were clearly distinguished (Maziewski *et al.*, 2012). One of the possible explanations for this induced PMA is that Co–Pt intermixing is forced by irradiation and the formation of the Co–Pt ordered alloy proceeds. Such a process was confirmed by Maziewski *et al.* (2012) and Lišková *et al.* (2012). Recent studies using the extended X-ray absorption fine-structure (EXAFS) technique

revealed that the enhancement of PMA in the moderate Ga⁺ fluence region was also related to in-plane lattice expansion of the Co film (Sakamaki *et al.*, 2012).

Identification of the roles of surface and of perimeter atoms in Co/Pt structures offers numerous possibilities for the engineering of magnetic moment strength and the anisotropy in fabricated nanostructures (Chappert *et al.*, 1998). Structures with PMA have potential applications in ultrahigh-density perpendicular recording (Stillrich *et al.*, 2010; Richter, 2007), magnetic ratchet memories (Franken *et al.*, 2012; Lambert *et al.*, 2013), magnetic field sensors (Matczak *et al.*, 2012) and controllable transport of magnetic beads (Tierno *et al.*, 2007). Hybrid systems are promising for the electric field control of magnetism in low-power spintronics devices (Lin *et al.*, 2013) or as spin injectors (Zarpellon *et al.*, 2012).

In the present paper we report the results of magneto-optical and synchrotron radiation studies of magnetic trilayers irradiated with a 30 keV Ga⁺ ion beam. A comparison of Pt/Co/Au and Pt/Co/Pt trilayers highlights the role of the top layer type in the interface intermixing responsible for the modification of magnetic properties, particularly PMA. The appearance of magnetic moments, owing to proximity effects for the atoms of nonmagnetic layers, is also discussed in detail.

2. Experimental details

Two types of epitaxial structures were grown, at room temperature, by a molecular beam epitaxy method on sapphire substrates: (a) cobalt wedge: Pt (20 nm)/Co wedge (0–5 nm)/[Pt (5 nm) or Au (5 nm)] and (b) cobalt flat samples: Pt (20 nm)/Co (3.3 nm)/[Pt (5 nm) or Au (5 nm)]. The deposition process was monitored *in situ* by reflection high-energy electron diffraction and Auger electron spectroscopy. Detailed information on the growth of the samples and orientation of the layers is given by Maziewski *et al.* (2012). Selection of Au as an alternative top layer should have a significant influence on the irradiation-induced magnetic properties owing to the difference in miscibility between Co/Pt (miscible) and Co/Au (immiscible) systems, and, consequently, their interface mixing under irradiation. The samples with the Co wedge were irradiated with 30 keV Ga⁺ ions with a fluence varying from 10¹³ up to 10¹⁶ ions cm^{−2} along a direction orthogonal to the Co wedge thickness gradient, similar to that reported by Maziewski *et al.* (2012). Thus, the Co wedge sample can be considered as an array of small uniform samples with variable Co thickness and irradiation fluence. After analysis of magnetic properties with a spatially resolved polar magneto-optical Kerr effect (PMOKE) technique, it is possible to present them as two-dimensional maps (d_{Co} , $\log F$) and select fluences F_1 and F_2 corresponding to the area with induced perpendicular magnetic anisotropy – branches 1 and 2 for a given Co thickness (Maziewski *et al.*, 2012). Further, these fluences, F_1 and F_2 , will be used for uniform irradiation of flat (constant Co thickness) large-area samples suitable for X-ray absorption spectroscopy (XAS) and X-ray magnetic circular dichroism (XMCD) study. The samples containing a flat cobalt layer and different capping layers were irradiated

with two fluences of $F_1 = 2.8 \times 10^{14}$ ions cm^{-2} (low) and $F_2 = 5.7 \times 10^{15}$ ions cm^{-2} (high) corresponding to the branches 1 and 2 for $d_{\text{Co}} = 3.3$ nm. TRIDYN (Möller *et al.*, 1988) simulations showed that: (a) in both types of sample systems the Ga^+ ions penetrate both Co layer interfaces and (b) the estimated etching depth is negligible for fluence F_1 and is a few nanometres for fluence F_2 .

Surface morphology was characterized with a commercial (NT-MDT) atomic force microscope (AFM) working in tapping mode at ambient conditions. In the case of a sharp boundary between irradiated and non-irradiated areas it also allows the depth of etching for a given fluence as a step height at the boundary to be measured.

Room-temperature PMOKE rotation hysteresis loops were measured with a magneto-optical set-up equipped with a laser diode (640 nm wavelength) giving a spot size of about 300 μm in diameter. A computer-controlled x - y scanning stage allowed the position of the laser spot on the sample surface to be selected. For a selected position, the PMOKE rotation hysteresis loop is measured sweeping magnetic field applied perpendicular to the sample surface. Analysis of these hysteresis loops enabled the determination of the main magnetic/magneto-optical parameters such as coercivity field, saturation field H_{SAT} , Kerr rotation maximum and zero field (remanence) values *etc.* The H_{SAT} field is equal to the effective magnetic anisotropy field for the film with in-plane magnetic anisotropy. These parameters maps on the (d_{Co} , $\log F$) plane were built for Co wedge samples (with Pt or Au coverage) irradiated with a fluence gradient, performed in a similar way by Maziewski *et al.* (2012).

XAS and XMCD spectra measured at the Co K -edge and Pt $L_{2,3}$ edges were obtained in the fluorescence mode at ID12 beamline of the ESRF, Grenoble. The measurements were performed at room temperature in an applied magnetic field of 0.6 T and in the glancing-incidence configurations (angle between the X-ray beam and the sample normal was equal to 79°). XAS spectra were averaged for two polarizations.

3. Results and discussion

The two-dimensional diagrams created on the basis of the measured PMOKE rotation hysteresis loops highlight the regions of the investigated samples with a specific direction of magnetization. These diagrams for saturation field H_{SAT} for (a) Pt/Co/Pt and (b) Pt/Co/Au trilayers as a function of d_{Co} , $\log F$ are presented in Fig. 1; similar to those presented by Maziewski *et al.* (2012).

The saturation field is defined for the part of the sample where the magnetization is oriented in the sample plane. It is equal to the value of the magnetic field applied in the perpendicular direction at which the magnetization reaches saturation along the field direction. Its value is represented by the color scale in Fig. 1. The part of the sample with perpendicular magnetization is marked in red. In our notation for that case the saturation field approaches to zero. On the right-hand side of Figs. 1(a) and 1(b) the vertical profiles of the saturation field, *i.e.* as a function of ion fluence, are presented

for a fixed Co layer thickness of $d_{\text{Co}} = 3.3$ nm. Contrary to the results obtained for the Pt/Co/Pt trilayer by Maziewski *et al.* (2012), only the second branch with PMA is well pronounced for Pt/Co/Au while the first one is visible only as a local increase of the saturation field. These differences are related to the various extents of Co mixing in the top Co/Pt and Co/Au interfaces. Also for higher fluences a transition to the super-

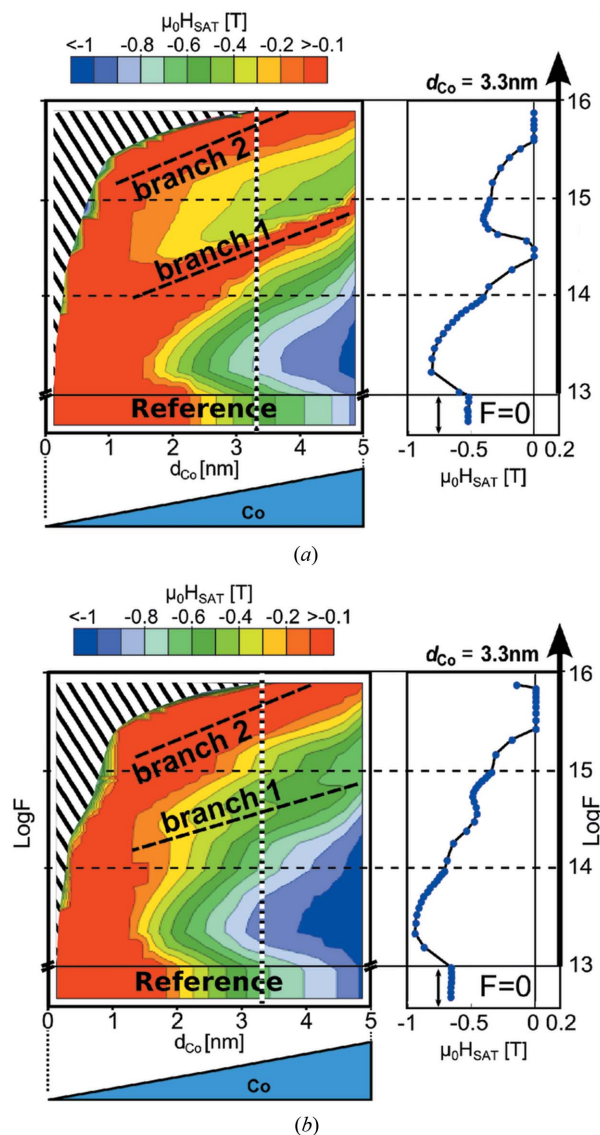


Figure 1

Two-dimensional diagrams (d_{Co} , $\log F$) of the saturation field H_{SAT} for Co wedge samples: (a) Pt/Co/Pt, (b) Pt/Co/Au. Thickness of Co layer d_{Co} is varied linearly along the x axis from 0 (left edge) to 5 nm (right edge). A schematic presentation of the Co layer profile is given at the bottom of the maps. The fluence of 30 keV Ga^+ irradiation is varied along the y axis from 10^{13} (at the bottom) up to 10^{16} ions cm^{-2} (at the top) perpendicular to the Co wedge direction. The value of fluence is given on a logarithmic scale on the right-hand side. A small lower part of the sample is not irradiated and marked as 'reference'. The regions with an enlarged value of perpendicular magnetic anisotropy are marked as 'branch 1' (low fluence) and 'branch 2' (high fluence). The superparamagnetic region (hatched area) is visible at the top left corner of the maps. The plots on the right-hand side of the diagrams correspond to the saturation field H_{SAT} changes along the black and white dashed vertical lines for $d_{\text{Co}} = 3.3$ nm. Samples are 10 mm \times 10 mm.

paramagnetic state takes place similar to those in Pt/Co/Pt structures. Moreover, the increase of the PMOKE rotation value under ion irradiation is slightly smaller than that reported by Maziewski *et al.* (2012). Our results indicate that a contribution of the top Co interface to magnetic changes induced by irradiation is dominant.

The uniform samples ($d_{\text{Co}} = 3.3$ nm) with a Au or a Pt capping layer, irradiated with fluences F_1 and F_2 corresponding to both branches, were measured using synchrotron radiation techniques. Figs. 2(a)–2(d) show the non-normalized XAS spectra measured at the Co K and the Pt L_3 absorption edges, for as-deposited samples and two irradiated ones with fluences F_1 and F_2 . For both systems (Figs. 2a and 2b) the shape of the non-normalized XAS Co K -edge absorption spectra for the as-deposited samples are typical of h.c.p. Co bulk structure (Kozinkin *et al.*, 2011). Upon irradiation the shapes of the spectra change. The features typical of pure metal are much less pronounced. These changes are probably related to the mixing of the layers at the interfaces which forces a modification of the $3d$ and $4p$ shells of the Co atoms. The electronic structure of transition metals is very sensitive to changes of their local environment. Abundance of Pt atoms in the nearest vicinity of Co atoms modifies their d and p shells due to hybridization with the d -states of Pt atoms. XAS spectra at the Co absorption edge for irradiated samples

resemble those obtained for the reference Co–Pt alloy (Lee *et al.*, 2003).

The shape of the non-normalized XAS spectra recorded at the L_3 platinum absorption edge also evolve after irradiation, see Figs. 2(c) and 2(d). The changes are slightly smaller than for Co; however, their origin is also related to the orbital hybridization. This confirms again the presence Co–Pt alloying in the samples irradiated with fluences F_1 and F_2 .

The observed evolution of the amplitude of the XAS spectra measured at the Co and Pt absorption edges with the applied ion fluence is a common feature of both studied systems, see Figs. 2(a)–2(b) and Figs. 2(c)–2(d), respectively. The amplitude is proportional to the number of absorbing atoms in the sample. For the non-irradiated sample and the irradiated one with fluence F_1 the amplitudes at the Co K -edge (see Fig. 2a) are similar, whereas for the fluence F_2 corresponding to branch 2 it drastically decreases. Such a behavior for the high fluence is related to the smaller amount of Co atoms remaining in the sample. Simple comparison between the spectra amplitudes show that the signal for the sample irradiated with the high fluence is about 45% less (1.8 times smaller) than for the as-deposited one. This means that almost half of the Co atoms were removed from the sample during the irradiation process. A similar behavior was observed for the Pt L_3 absorption edge (Fig. 2c). However, the decrease by

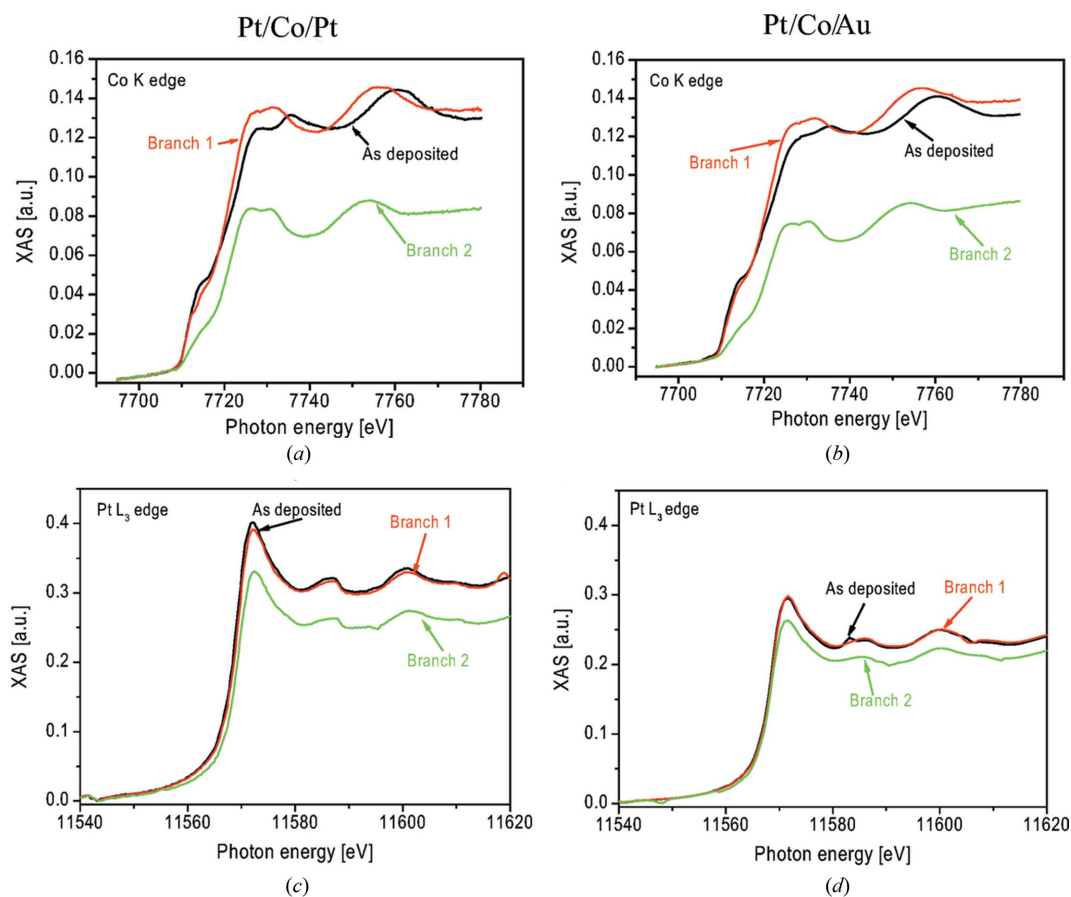
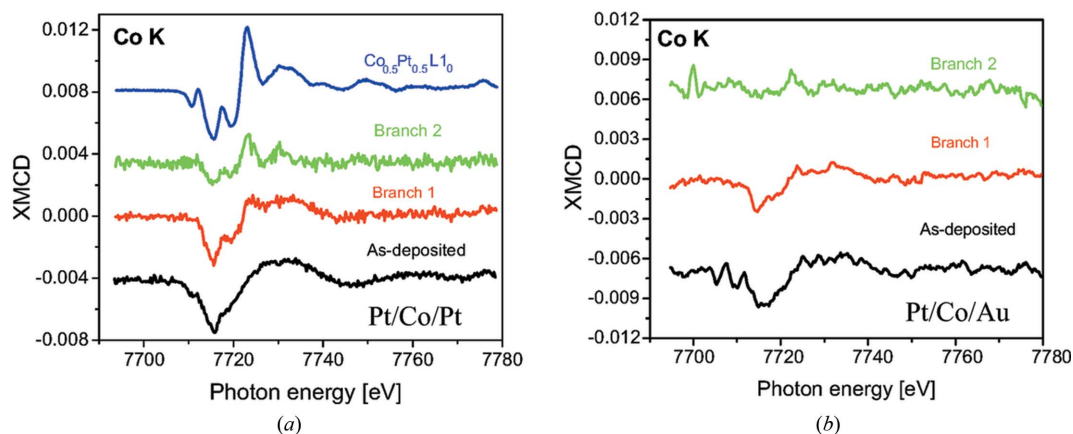


Figure 2

XAS spectra of three types of samples for Pt/Co/Pt and Pt/Co/Au trilayers: as-deposited and two irradiated with fluences F_1 and F_2 corresponding to the branches 1 and 2, respectively: (a)–(b) non-normalized XAS spectra at the Co K -edge, (c)–(d) non-normalized XAS spectra on the Pt L_3 -edge.


Figure 3

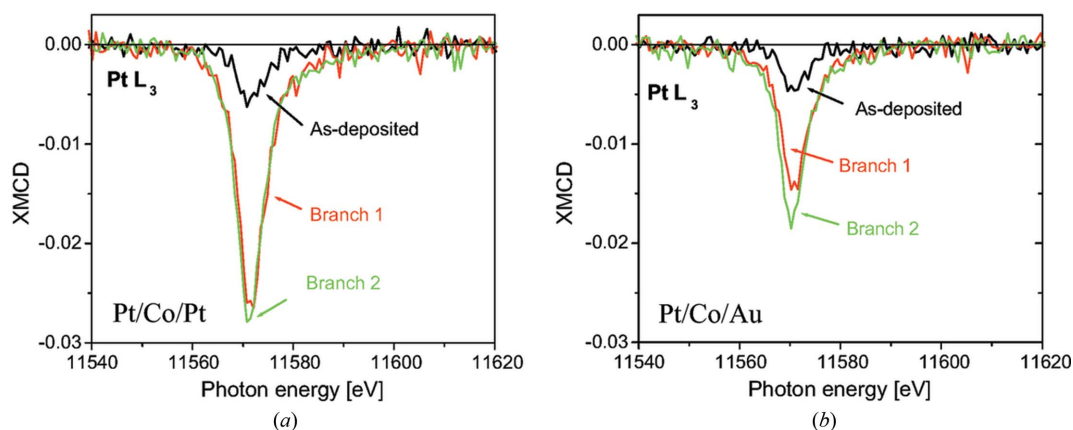
Co *K*-edge XMCD spectra of the samples for (a) Pt/Co/Pt and (b) Pt/Co/Au trilayers: as-deposited and two irradiated with fluences F_1 and F_2 corresponding to the branches 1 and 2, respectively. Spectra are shifted vertically for clarity. For comparison, the XMCD spectrum for the $\text{Co}_{0.5}\text{Pt}_{0.5}$ L₁₀ ordered alloy is also presented (a).

18% is much smaller in comparison with Co (1.2 times smaller). This difference is related with initially different amounts of the Co and Pt atoms in the sample. The decrease of amplitude might be used for a simple estimation of the sample etching effects under irradiation. Thus, irradiation with the high fluence removes about 5 nm of Pt and about 1.9 nm of Co. Obtained values are in good agreement with the step height of 7.5 nm in the sample topography between non-irradiated and irradiated with fluence F_2 regions measured with an AFM. A similar qualitative step height reduction with ion fluence was observed for Pt/Co/Au samples. However, quantitative differences result from different sputtering yields of the capping Pt and Au layers.

Figs. 3(a) and 3(b) show the XMCD spectra obtained at the Co *K*-edge for Pt/Co/Pt and Pt/Co/Au trilayers, respectively. For non-irradiated samples of both systems the spectra are very similar to each other and resemble the XMCD spectrum recorded for a pure h.c.p. Co layer (Stähler *et al.*, 1993). It is possible to distinguish two additional peaks (emerging at 7716 and 7727 eV) for the samples irradiated with the fluences F_1 and F_2 . The shape of the spectra acquired for both branches

resemble the reference XMCD spectrum measured for the $\text{Co}_{0.5}\text{Pt}_{0.5}$ alloy with well developed L₁₀ structure (topmost one in Fig. 3a). Such coincidence is a strong indication that the Co–Pt alloy is formed and responsible for the enhanced perpendicular anisotropy in branches 1 and 2. It is also worth mentioning that in the irradiated Pt/Co/Au trilayer a possible mixing of Co and Au does not contribute to modifications of the XMCD spectrum. Additional features come mainly from the Co/Pt interface due to intermixing/alloying.

The XMCD spectra measured at the platinum *L*₃ absorption edge for both types of the samples are presented in Figs. 4(a)–4(b). The amplitudes of the spectra are much higher for the samples irradiated with fluences F_1 and F_2 than for the as-deposited one. The increased amplitude reflects the appearance of magnetic moments at the Pt atoms which are induced by the magnetic moments of adjacent Co atoms in the alloy formed. Electron hybridization and the resulting changes in the density of states at the Fermi level are responsible for the observed properties of the Pt atoms. Similarly to the Co *K*-edge samples, the amplitude for the irradiated samples in the Pt/Co/Au trilayer is lower than that for the Pt/Co/Pt one.


Figure 4

XMCD spectra of the three types of sample for trilayers (a) Pt/Co/Pt and (b) Pt/Co/Au: as-deposited and two irradiated with fluences F_1 and F_2 corresponding to both branches with changed saturation field at the Pt *L*₃ absorption edge.

Table 1
Spin and orbital magnetic moment induced on Pt atoms in Pt/Co/Pt and Pt/Co/Au trilayers.

	Pt/Co/Pt			Pt/Co/Au		
	μ_L ($\mu\text{B atom}^{-1}$)	μ_S ($\mu\text{B atom}^{-1}$)	μ_L/μ_S	μ_L ($\mu\text{B atom}^{-1}$)	μ_S ($\mu\text{B atom}^{-1}$)	μ_L/μ_S
Branch 1	0.012	0.073	0.164	0.0069	0.042	0.164
Branch 2	0.019	0.084	0.226	0.013	0.056	0.232

This difference is related to the smaller number of Pt atoms adjacent to Co in the Au/Co/Pt system as only at one interface does Co–Pt alloying take place.

Using the sum rules (Thole *et al.*, 1992), the spin and orbital magnetic moments of the Pt atoms in the Pt/Co/Pt and the Pt/Co/Au trilayers for the as-deposited samples and two irradiated ones were determined. As the XMCD spectra at the Pt L_3 absorption edge for both as-deposited samples are very similar, we assumed that the relation μ_L/μ_S for Pt is identical. Under this assumption the following moments were obtained: $\mu_L = 0.002 \mu\text{B}$ per atom and $\mu_S = 0.021 \mu\text{B}$ per atom and $\mu_L/\mu_S = 0.095$. The calculated values of the induced moments at Pt atoms for irradiated samples are presented in Table 1. The increase of the spin and orbital magnetic moments in both systems with respect to the non-irradiated structures is very clear. The moments at the Pt atoms in Pt/Co/Au are slightly smaller than in Pt/Co/Pt. This is probably related to the above-mentioned different number of Pt atoms in the Co neighborhood. In both irradiated systems the orbital moment, in particular, is larger by an order of magnitude in comparison with the as-deposited configuration.

The observed increase of the magnetic moments at Pt atoms shows an enhanced mixing at the interfaces which results in a greater number of Co atoms adjacent to Pt ones while the Pt matrix crystallinity is still maintained. Rearrangements of this kind also change the magnetic moments at Co atoms and magnetic anisotropy energy while these parameters strongly depend on the local atomic coordination (Gambardella *et al.*, 2003).

4. Summary

XAS and XMCD studies of the magnetic properties of Pt/Co/Pt and Pt/Co/Au trilayers upon 30 keV Ga^+ ion irradiation highlight the intermixing processes at the interfaces. Additionally, two-dimensional diagrams of magnetic parameters as a function of Co layer thickness and applied ion fluence, obtained from magneto-optical investigations, enable the comparison of magnetic anisotropy spatial distribution in Pt/Co/Au and Pt/Co/Pt trilayers upon irradiation. In the Pt/Co/Au trilayer, the irradiation induces two branches: the first one with only an increased value of the saturation field and the second one with PMA. In the Pt/Co/Pt trilayer, two branches with PMA are very well distinguished. The shape of the XAS spectra measured at both Co K and Pt L_3 absorption edges upon ion irradiation in both systems were changed in comparison with the as-deposited configurations. The observed evolution is related to changes in the local environment of the absorbing atoms.

The decrease in the amplitude of the XAS spectra for the highest irradiation fluence at both Co and Pt absorption edges is related to material removal (sputtering) during the irradiation process. XMCD spectra at the Co K -edge for irradiated samples are similar to XMCD spectra obtained for the Co–Pt reference alloy.

This is evidence for intermixing at the interfaces and the creation of a Co–Pt alloy. Such an explanation is confirmed by magnetic moments induced at Pt atoms, especially by the enhanced increase of the orbital moments determined from the sum rules. The mixing of Co and Pt atoms and the resulting alloy creation are responsible for the formation of branches with modified values of the saturation field and particularly with PMA in two-dimensional diagrams. Comparison of both Pt/Co/Pt and Pt/Co/Au trilayers shows additionally the influence of the top interface on induced magnetic properties: one branch with only increased values of the saturation field and smaller values of induced magnetic moment at Pt atoms. In Pt/Co/Au trilayers, the bottom of the Co/Pt interface is mainly responsible for the induced changes.

Acknowledgements

Supported by following projects: SYMPHONY project operated within the Foundation for Polish Science Team Programme co-financed by the EU European Regional Development Fund, OPIE2007–2013, Preludium financed by the National Science Centre (2011/03/N/ST3/02408), and bilateral Polish–French Polonium.

References

Bandiera, S., Sousa, R. C., Rodmacq, B. & Dieny, B. (2011). *IEEE Magn. Lett.* **2**, 3000504.
 Bandiera, S., Sousa, R. C., Rodmacq, B. & Dieny, B. (2012). *Appl. Phys. Lett.* **100**, 142410.
 Bartolome, J., Garcia, L. M., Bartolome, F., Luis, F., Petroff, F., Deranlot, C., Wilhelm, F. & Rogalev, A. (2007). *J. Magn. Mater.* **316**, e9–e12.
 Brandle, H., Weller, D., Scott, J. C., Parking, S. S. P. & Lin, C.-J. (1992). *IEEE Trans. Magn.* **28**, 2967–2969.
 Chappert, C., Bernas, H., Ferre, J., Kottler, V., Jamet, J.-P., Chen, Y., Cambril, E., Devolder, T., Rousseaues, F., Mathet, V. & Launois, H. (1998). *Science*, **280**, 1919–1922.
 Chappert, C. & Bruno, P. (1988). *J. Appl. Phys.* **64**, 5736.
 Chowdhury, P., Kulkarni, P. D., Krishnan, M., Barshilia, H. C., Sagdeo, A., Rai, S. K., Lodha, G. S. & Sridhara Rao, D. V. (2012). *J. Appl. Phys.* **112**, 023912.
 Fowley, C., Diao, Z., Faulkner, C. C., Kally, J., Ackland, K., Behan, G., Zhang, H. Z., Deac, A. M. & Coey, J. M. D. (2013). *J. Phys. D*, **46**, 195501.
 Franken, J. H., Swagten, H. J. M. & Koopmans, B. (2012). *Nat. Nanotech.* **7**, 499–503.
 Gambardella, P., Rusponi, S., Veronese, M., Dhési, S. S., Grazioli, C., Dallmeyer, A., Cabria, I., Zeller, R., Dederichs, P. H., Kern, K., Carbone, C. & Brune, H. (2003). *Science*, **300**, 1130–1133.
 Jaworowicz, J., Maziewski, A., Mazalski, P., Kisielewski, M., Sveklo, I., Tekielak, M., Zablotkii, V., Ferré, J., Vernier, N., Mougín, A., Henschke, A. & Fassbender, J. (2009). *Appl. Phys. Lett.* **95**, 022502.
 Knepper, J. W. & Yang, F. Y. (2005). *Phys. Rev. B*, **71**, 224403.

- Kozinkin, Yu. A., Novakovich, A. A., Kozinkin, A. V., Vedrinskii, R. V., Zubavichus, Ya. V. & Veligzhanin, A. A. (2011). *Phys. Solid State*, **53**, 1–5.
- Kuswik, P., Sveklo, I., Szymanski, B., Urbaniak, M., Stobiecki, F., Ehresmann, A., Engel, D., Mazalski, P., Maziewski, A. & Jagielski, J. (2011). *Nanotechnology*, **22**, 095303.
- Lambert, C. H., Rajanikanth, A., Hauet, T., Mangin, S., Fullerton, E. E. & Andrieu, S. (2013). *Appl. Phys. Lett.* **102**, 122410.
- Lee, T. Y., Son, D. S., Lim, S. H. & Lee, S. R. (2013). *J. Appl. Phys.* **113**, 216102.
- Lee, Y. S., Rhee, J. Y., Whang, C. N. & Lee, Y. P. (2003). *Phys. Rev. B*, **68**, 235111.
- Lehnert, A., Dennler, S., Błoński, P., Rusponi, S., Etzkorn, M., Moulas, G., Bencok, P., Gambardella, P., Brune, H. & Hafner, J. (2010). *Phys. Rev. B*, **82**, 094409.
- Lin, W., Lei, N., Vernier, N., Agnus, G., Adam, J.-P., Eimer, S., Devolder, T., Lecoœur, P. & Ravelosona, D. (2013). *Thin Solid Films*, **533**, 70–74.
- Lišková, E., Veis, M., Višňovský, S., Ferré, J., Mougín, A., Mazalski, P., Maziewski, A., Liedke, M. O. & Fassbender, J. (2012). *Thin Solid Films*, **520**, 7169–7172.
- Manchon, A., Pizzini, S., Vogel, J., Uhlir, V., Lombard, L., Ducret, C., Auffret, S., Rodmacq, B., Dieny, B., Hochstrasser, M. & Panaccione, G. (2008). *J. Magn. Magn. Mater.* **320**, 1889.
- Matczak, M., Kuświk, P., Szymański, B., Urbaniak, M., Schmidt, M., Aleksiejew, J., Stobiecki, F. & Ehresmann, A. (2012). *Appl. Phys. Lett.* **100**, 162402.
- Mazalski, P., Kurant, Z., Maziewski, A., Liedke, M. O., Fassbender, J., Baczewski, L. T. & Wawro, A. (2013). *J. Appl. Phys.* **113**, 17C109.
- Maziewski, A., Mazalski, P., Kurant, Z., Liedke, M. O., McCord, J., Fassbender, J., Ferré, J., Mougín, A., Wawro, A., Baczewski, L. T., Rogalev, A., Wilhelm, F. & Gemming, T. (2012). *Phys. Rev. B*, **85**, 054427.
- Mihai, A. P., Whiteside, A. L., Canwell, E. J., Marrows, C. H., Benitez, M. J., McGrouther, D., McVitie, S., McFadzean, S. & Moore, A. (2013). *Appl. Phys. Lett.* **103**, 262401.
- Möller, W., Eckstein, W. & Biersack, J. P. (1988). *Comput. Phys. Commun.* **51**, 355–368.
- Nistor, C., Balashov, T., Kavich, J. J., Lodi Rizzini, A., Ballesteros, B., Gaudin, G., Auffret, S., Rodmacq, B., Dhesi, S. S. & Gambardella, P. (2011). *Phys. Rev. B*, **84**, 054464.
- Pouloupoulos, P., Angelakeris, M., Papaioannou, E. Th., Flevaris, N. K., Niarchos, D., Nyvlt, M., Prosser, V., Visnovsky, S., Mueller, Ch., Fumagalli, P., Wilhelm, F. & Rogalev, A. (2003). *J. Appl. Phys.* **94**, 7662.
- Rettnner, C. T., Anders, S., Baglin, J. E. E., Thomson, T. & Terris, B. D. (2002). *Appl. Phys. Lett.* **80**, 279.
- Richter, H. J. (2007). *J. Phys. D*, **40**, R149–R177.
- Sakamaki, M., Amemiya, K., Liedke, M. O., Fassbender, J., Mazalski, P., Sveklo, I. & Maziewski, A. (2012). *Phys. Rev. B*, **86**, 024418.
- Schaller, D. M., Bürgler, D., Schmidt, C. M., Meisinger, F. & Güntherodt, H. J. (1999). *Phys. Rev. B*, **59**, 14516–14519.
- Stähler, S., Schütz, G. & Ebert, H. (1993). *Phys. Rev. B*, **47**, 818–826.
- Stillrich, H., Menk, C., Froemter, R. & Oepen, H. P. (2010). *J. Magn. Magn. Mater.* **322**, 1353.
- Thole, B. T., Carra, P., Sette, F. & van der Laan, G. (1992). *Phys. Rev. Lett.* **68**, 1943–1946.
- Tierno, P., Reddy, S. V., Yuan, J., Johansen, T. H. & Fischer, T. M. (2007). *J. Phys. Chem. B*, **111**, 13479–13482.
- Vieu, C., Gierak, J., Launois, H., Aign, T., Meyer, P., Jamet, J. P., Ferré, J., Chappert, C., Devolder, T., Mathet, V. & Bernas, H. (2002). *J. Appl. Phys.* **91**, 3103.
- Zarpellon, J., Jaffrès, H., Frougier, J., Deranlot, C., George, J. M., Mosca, D. H., Lemaître, A., Freimuth, F., Duong, Q. H., Renucci, P. & Marie, X. (2012). *Phys. Rev. B*, **86**, 205314.
- Zhang, J. Y., Wu, Z. L., Wang, S. G., Zhao, C. J., Yang, G., Zhang, S. L., Liu, Y., Liu, S., Teng, J. & Yu, G. H. (2013). *Appl. Phys. Lett.* **102**, 102404.
- Zhang, J., Yang, G., Wang, S., Zhang, S., Zhang, P., Cao, X., Jiang, S., Zhao, C., Liu, Y., Wang, H. & Yu, G. (2013). *Appl. Phys. Express*, **6**, 103007.